Malaysian Journal of Chemistry, 2024, Vol. 26(5), 209-220
(Special Issue: *3rd Virtual International Symposium on Sciences 2023*)

Revisiting the Reaction of $Ru_3(CO)_{12}$ with $Ph_2PCH_2CH_2PPh_2$: Synthesis, Crystal Structure, and DFT Study of $Ru_3(CO)_8(\mu\text{-}Ph_2PCH_2CH_2PPh_2)_2$

Husna Izzati Muhammad Nor Azharan[1], Muhamad Azwan Hamali[2], Amalina Mohd Tajuddin[2,3], Suhaila Sapari[4], Fazira Ilyana Abdul Razak[4], Noor Hidayah Pungot[5], Shahrul Nizam Ahmad[2] and Siti Syaida Sirat[1,3]*

[1]Faculty of Applied Sciences, Universiti Teknologi MARA, Cawangan Negeri Sembilan, Kampus Kuala Pilah, 72000 Kuala Pilah, Negeri Sembilan, Malaysia
[2]Faculty of Applied Sciences, Universiti Teknologi MARA, 40450 Shah Alam, Selangor, Malaysia
[3]Atta-ur-Rahman Institute for Natural Product Discovery (AuRIns), Universiti Teknologi MARA, Kampus Puncak Alam, 42300 Bandar Puncak Alam, Selangor, Malaysia
[4]Faculty of Science, Universiti Teknologi Malaysia, 81300 Skudai, Johor Bahru, Malaysia
[5]Organic Synthesis Research Laboratory, Institute of Science, Universiti Teknologi MARA, 42300 Bandar Puncak Alam, Selangor, Malaysia
*Corresponding author (e-mail: sitisyaida@uitm.edu.my)

The reaction between $Ru_3(CO)_{12}$ and 1,2-bis(diphenylphosphino)ethane (dppe/ $Ph_2PCH_2CH_2PPh_2$) with the presence of sodium benzophenone ketyl radical anion in tetrahydrofuran resulted in the formation of the expected metal cluster $Ru_3(CO)_8(\mu\text{-}Ph_2PCH_2CH_2PPh_2)_2$. The compound was completely characterised by spectroscopic methods, and its molecular structure was confirmed by single-crystal X-ray diffraction. The structure of $Ru_3(CO)_8(\mu\text{-}Ph_2PCH_2CH_2PPh_2)_2$ was crystallised in triclinic system with *P*-1 group at a = 14.558(3), b = 18.869(5), c = 19.088(4) Å, α = 89.809(6), $ß$ = 89.979(5) and γ = 89.968(6)°. The $Ph_2PCH_2CH_2PPh_2$ ligands are coordinated with μ_2-η^2 bonding mode to Ru–Ru bonds. The structure was further analysed by Density Functional Theory (DFT) using hybrid GEN method exchange-correlation LanL2DZ for Ru metal and B3LYP/6-31G (d, p) basis set for all other atoms. The HOMO-LUMO energy gap and the Molecular Electrostatic Potential (MEP) were illustrated.

Keywords: Triruthenium, metal cluster; diphosphine ligand; DFT

Received: November 2023; Accepted: February 2024

There is an enormous amount of research on the chemistry of transition metal carbonyl clusters [1-3], however, there is little information available on the structure of $Ru_3(CO)_8(L\text{-}L)_2$ where L-L = diphosphine ligands. Some of the reported structures only include L-L= dppm (bis(diphenylphosphino)methane) [4], dppa (bis(diphenylphosphino)amine) [5], dcpm (bis (dicyclohexylphosphino)methane), and F-dppe (1,2-bis[bis-pentafluorophenyl) phosphino]ethane) [6]. Transition metal carbonyl clusters have become the topic of numerous studies due to their potential as catalysts for a variety of organic reactions, including hydroformylation reactions [6-8]. In 1982, Bruce and coworkers reported on the reaction of 1,2-bis(diphenylphosphino)ethane ($Ph_2PCH_2CH_2PPh_2$) with $Ru_3(CO)_{12}$ under mild synthesis reaction in tetrahydrofuran (THF) [9]. The study reported on the approach of different reaction ratios of $Ru_3(CO)_{12}$ and $Ph_2PCH_2CH_2PPh_2$ with the formation of $[Ru_3(CO)_{11}]_2(\eta\text{-}Ph_2PCH_2CH_2PPh_2)$, $Ru_3(CO)_{11}(\eta^1\text{-}Ph_2PCH_2CH_2PPh_2)$, $Ru_3(CO)_{10}(\mu\text{-}Ph_2PCH_2CH_2PPh_2)$ and $Ru_3(CO)_8(\mu\text{-}Ph_2PCH_2CH_2PPh_2)_2$. All structures were elucidated using IR and elemental analysis with comparison to those of similar structures previously reported. Only the structure of $Ru_3(CO)_{10}(\mu\text{-}Ph_2PCH_2CH_2PPh_2)$ has been successfully determined by single-crystal X-ray Diffraction [9]. There is no reported crystal structure on $Ru_3(CO)_8(\mu\text{-}Ph_2PCH_2CH_2PPh_2)_2$. Thus, our interest is to characterise *via* spectroscopic methods and study the molecular structure of $Ru_3(CO)_8(\mu\text{-}Ph_2PCH_2CH_2PPh_2)_2$.

Previously, the crystal structures of $Ru_3(CO)_8(\mu\text{-dcpm})_2$ and $Ru_3(CO)_8(\text{F-dppe})_2$ have been reported and the bonding mode of the coordinated diphosphine ligand was found to be different, although the number of substituted carbonyl is similar. The structure of $Ru_3(CO)_8(\mu\text{-dcpm})_2$ is the same as that of $Ru_3(CO)_8(\mu\text{-dppm})_2$ and follows the normal μ_2-η^2 bonding mode [4,6]. However, in $Ru_3(CO)_8(\text{F-dppe})_2$, one F-dppe ligand is μ_2-η^2 bonded to the Ru-Ru bond and the second F-dppe ligand is bonded by μ_1-η^2 coordination to the third ruthenium atom [6]. Recent studies also revealed that the crystal structure of triosmium cluster carbonyl derivative, $Os_3(CO)_8(dppe)_2$ has a similar coordinated ligand as that of $Ru_3(CO)_8(\text{F-dppe})_2$ [3]. It was proposed that there are three potential coordinations for carbonyl substitution in triosmium

†Paper presented at the 3rd Virtual International Symposium on Sciences (3rd VISoS 2023)

cluster derivatives, two of which are stated as: one has both bidentate ligands bonded to the Os–Os bond by a bridging mode. The other has one ligand bridged to Os1 and Os2, while another chelated to Os3 [3]. Thus, it is significant to analyse the bonding mode of diphosphine ligand ($Ph_2PCH_2CH_2PPh_2$) on Ru-Ru bond in $Ru_3(CO)_8(L\text{-}L)_2$ structure type.

In this study, we focused on the synthesis and characterise of the titled compound, $Ru_3(CO)_8(\mu\text{-}Ph_2PCH_2CH_2PPh_2)_2$ also known as, $Ru_3(CO)_8(\mu\text{-}dppe)_2$ that was previously reported by Bruce and co-workers in 1982 [9]. In addition, the geometrical structure of the successfully obtained crystal are analysed. The crystallographic analysis and DFT investigations of $Ru_3(CO)_8(\mu\text{-}Ph_2PCH_2CH_2PPh_2)_2$ are also described.

EXPERIMENTAL

Chemicals and Materials

All reactions were carried out in an inert environment, under nitrogen gas. Prior to use, reagent grade solvents, tetrahydrofuran (THF) were dried and distilled by standard procedures. Other solvents were used as in analytical research grade (AR) solvents. The following chemicals: $Ru_3(CO)_{12}$ (Sigma Aldrich), $Ph_2PCH_2CH_2PPh_2$ (Sigma Aldrich) were used without additional purification.

Characterisation

Infrared spectra were recorded using a solid sample on the Attenuated Total Reflectance Fourier Transform Infrared (ATR-FTIR) spectroscopy on Perkin-Elmer FT-IR 1600 spectrometer. ^{1}H NMR spectra were recorded on Jeol ECZS400 MHz spectrometer. ^{31}P NMR spectra were recorded on Bruker Avance 400 MHz spectrometer. Preparative Thin Layer Chromatography (TLC) was performed on glass plates (20 × 20 cm) coated with 0.5 mm Silica Gel (Merck, 60GF254).

Synthesis of $Ru_3(CO)_8(\mu\text{-}Ph_2PCH_2CH_2PPh_2)_2$

$Ru_3(CO)_{12}$ (100 mg, 0.156 mmol) and $Ph_2PCH_2CH_2PPh_2$ (124.6 mg, 0.313 mmol) were mixed in 25 mL distilled THF according to a reported method [9] under an inert, nitrogen atmosphere. A few drops of sodium benzophenone ketyl radical anion was added, and the solution was stirred at room temperature for 60 minutes. The completion of the reaction was monitored *via* TLC analysis. The solvent removal was performed under vacuum, and all products were isolated with elution 2:3 (dichloromethane: *n*-hexane) by preparative TLC. The separation afforded four bands, with two significant bands that were collected. The other bands were in trace amount and not characterised. The first band gave $Ru_3(CO)_{10}(\mu\text{-}Ph_2PCH_2CH_2PPh_2)$ (R_f = 0.75). and the third band afforded the titled compound, $Ru_3(CO)_8(\mu\text{-}Ph_2\ PCH_2\ CH_2PPh_2)_2$. ($R_f$ = 0.50). Yield: 13.28%. IR (dichloromethane) ν(CO): 2055s, 2024m, 1982vs cm^{-1}. ^{1}H 400 MHz NMR ($CDCl_3$): δ 7.51-7.42 (m, 40H, Ph), 2.22-2.16 (m,8H,CH_2); ^{31}P{^{1}H} 400MHz NMR ($CDCl_3$): δ 62.16 (s, $Ph_2PCH_2CH_2PPh_2$), δ 38.36 (s, $Ph_2PCH_2CH_2PPh_2$). Single crystals suitable for X-ray crystallography were grown by solvent-solvent diffusion of dichloromethane/*n*-hexane at 10 ˚C.

Crystallographic Analysis

Crystallographic analysis were carried out with Bruker D8 QUEST CCD diffractometer equipped with Photon III detector and graphite-monochromated Mo-Kα radiation (λ = 0.71069Å) at 298 K. The frames were recorded using ϕ and ω scan method and the intensities were integrated with the Bruker SAINT software package [10]. Using Olex2 [11], the structure was solved by direct method using SHELXS [12] and refined by full-matrix least squares on F^2 using the SHELXL [13] software package. All non-hydrogen atoms were treated anisotropically, while all hydrogen atoms were assigned to calculated positions using a riding model with appropriately fixed isotropic thermal parameters refined isotropically. The graphical representation of the crystal structure was plotted using Mercury software [14]. PLATON program was used for the molecular structure calculation [15]. The crystallographic and structure refinement data of $Ru_3(CO)_8(\mu\text{-}Ph_2PCH_2CH_2PPh_2)_2$ are shown in Table 1.

Table 1. Data and structure refinement for $Ru_3(CO)_8(\mu\text{-}Ph_2PCH_2CH_2PPh_2)_2$.

	Description
CCDC No.	CCDC2297431
Empirical formula	$C_{60}H_{48}O_8P_4Ru_3$
Formula weight (g mol^{-1})	1324.07
Temperature (K)	296.3
Crystal system	triclinic
Space group	*P*-1
a (Å)	14.558 (3)

b (Å)	18.869 (5)
c (Å)	19.088 (5)
α (°)	89.809 (6)
β (°)	89.979 (5)
γ (°)	89.968 (6)
Volume (Å^3)	5243 (2)
Z	2
ρ_{calc} (g cm^3)	1.677
F (000)	2656.0
Absorption coefficient (mm^{-1})	1.033
Crystal size (mm^3)	0.329 × 0.269 × 0.073
θ Range (°)	1.067 to 25.283
Reflections collected/unique	117699
R_{int}	25.16
Data/restrains/parameter	18797/20/463
Goodness-of fit on F^2	1.720
Final R indices [$F^2>2\sigma(F^2)$]	R_1 = 0.2319, wR_2 = 0.5534
Largest difference in peak and hole (e Å^{-3})	2.61/-1.97

$w = 1/[\sigma^2(F_o^2) + (0.0214P)^2+124.9806P]$, where $P = (F_o^2 + 2F_c^2)/3$; [a] $R = \Sigma||F_o| - |F_c||/\Sigma|F_o|$, [b] $wR = \{w\Sigma(|F_o| - |F_c|)^2/\Sigma w|F_o|^2\}\}^{1/2}$, [c] $GOF = \{\Sigma w(|F_o| - |F_c|)^2/(n–p)\}^{1/2}$, where *n* is the number of reflections and *p is* the total number of parameters refined.

Density Functional Theory (DFT)

DFT calculations were performed using Gaussian16 (Gaussian Inc., Wallingford, CT, USA) [16] and Gaussview6 (Semichem, Inc., Shawnee Mission, KS, USA) [17] software was used to visualise the structure. The calculation was performed using the data crystal from single crystal X-ray diffraction. The calculation used hybrid GEN method exchange -correlation LanL2DZ for Ru metal and B3LYP/6-31G (d, p) basis set for all other atoms [18-21]. Harmonic frequency calculations were performed at the same level of theory without any imaginary frequencies.

RESULTS AND DISCUSSION

Synthesis and Characterisation of $Ru_3(CO)_8(\mu\text{-}Ph_2PCH_2CH_2PPh_2)_2$

$Ru_3(CO)_8(\mu\text{-}Ph_2PCH_2CH_2PPh_2)_2$ was synthesised utilising 1:2 molar ratio of $Ru_3(CO)_{12}$ and $Ph_2PCH_2CH_2PPh_2$ in THF with sodium benzophenone ketyl radical anion as the initiator. The carbonyl substitution occurred with two bidentate $Ph_2PCH_2CH_2PPh_2$ ligands linked to the metal cluster on both sides of the structure. The orange solution of $Ru_3(CO)_8(\mu\text{-}Ph_2PCH_2CH_2PPh_2)_2$ was isolated *via* preparative TLC and characterised by FTIR, ^{1}H, and $^{31}P\{^1H\}$ NMR spectroscopy. The stretching carbonyl was observed in the IR spectrum of $Ru_3(CO)_8(\mu\text{-}Ph_2PCH_2CH_2PPh_2)_2$ at 2055s, 2024m, and 1982vs cm^{-1}. These values gave a similar pattern of values as that of in $Ru_3(CO)_8(L\text{-}L)_2$ series, in which L-L=diphosphine ligand. [4-6]. In the ^{1}H NMR spectrum, there are aromatic protons appeared as multiplet peaks at 7.51-7.42 ppm and a multiplet of methylene proton in the ligand $Ph_2PCH_2CH_2PPh_2$ at 2.22-2.16 ppm. The ^{31}P NMR spectrum shows two singlet peaks at 62.16 ppm and 38.36 ppm of $Ph_2PCH_2CH_2PPh_2$ ligand.

Crystal Structure of $Ru_3(CO)_8(\mu\text{-}Ph_2PCH_2CH_2PPh_2)_2$

The crystal structure of $Ru_3(CO)_8(\mu\text{-}Ph_2PCH_2CH_2PPh_2)_2$ was found to be in triclinic *P*-1 space group in which *a* = 14.558 (3) *b* = 18.869 (5), *c* = 19.088 (5) Å = 89.809 (6), *ß* =89.979 (5) and *γ* = 89.968. There are two asymmetric units of $Ru_3(CO)_8(\mu\text{-}Ph_2PCH_2CH_2PPh_2)_2$ in one unit cell, visualised as molecule A and molecule B. Figure 1 shows the molecular structure of only one molecule, and the other has been omitted for clarity. Figure 1 (a) shows the ORTEP diagram of $Ru_3(CO)_8$ $(\mu\text{-}Ph_2PCH_2CH_2PPh_2)_2$ from the single crystal XRD.

The bidentate ligand, $Ph_2PCH_2CH_2PPh_2$ was found to be bridged to the Ru1–Ru2, and Ru1–Ru3 atoms at the equatorial position. Figure 2 shows the Ru–Ru bond length values of $Ru_3(CO)_{12}$, $Ru_3(CO)_{10}$ $(\mu\text{-}Ph_2PCH_2CH_2PPh_2)$, and $Ru_3(CO)_8(\mu\text{-}Ph_2PCH_2CH_2PPh_2)_2$. The average Ru–Ru bond lengths of $Ru_3(CO)_8$ $(\mu\text{-}Ph_2PCH_2CH_2PPh_2)_2$ were found to be 2.8257 Å (molecule A), and 2.8287 Å (molecule B). These values are comparable to those of the Ru–Ru bonds of the parent compound, $Ru_3(CO)_{12}$ [2.8542 Å] [22] and $Ru_3(CO)_{10}(\mu\text{-}Ph_2PCH_2CH_2PPh_2)$ [2.8527Å]. There is one shorter Ru–Ru bond than the other two bonds in $Ru_3(CO)_8(\mu\text{-}Ph_2PCH_2CH_2PPh_2)_2$, which is the unbridged

Ru2–Ru3 bond [molecule A=2.748(4)Å; molecule B= 2.754(4)Å]. Similar observations can also been seen with $Ru_3(CO)_8(dcpm)_2$ [Ru2–Ru3= 2.8422(4) Å] [6] and $Ru_3(CO)_8(dppa)_2$ [Ru2-Ru3= 2.8223(13) Å] [5]. This pattern is in contrast to the study found in $Ru_3(CO)_8(dppm)_2$ where the unbridged Ru2–Ru3 (2.858(2) Å) was found to be the longest compared to the bridged Ru–Ru bond (Ru1–Ru2 = 2.826(2) Å, Ru1–Ru3= 2.833(2) Å) [4]. This might be due to the strain in the dppm ligand [23], causing the unbridged bond to have a less significant effect on the Ru–Ru bond. In the case of other similar compounds such as $Ru_3(CO)_8(\mu\text{-}Ph_2PCH_2CH_2PPh_2)_2$, the bulkiness of the ligand causes the shortening effect on the bond that is not bridged by the ligand, in order to overcome the steric effect of the ligand.

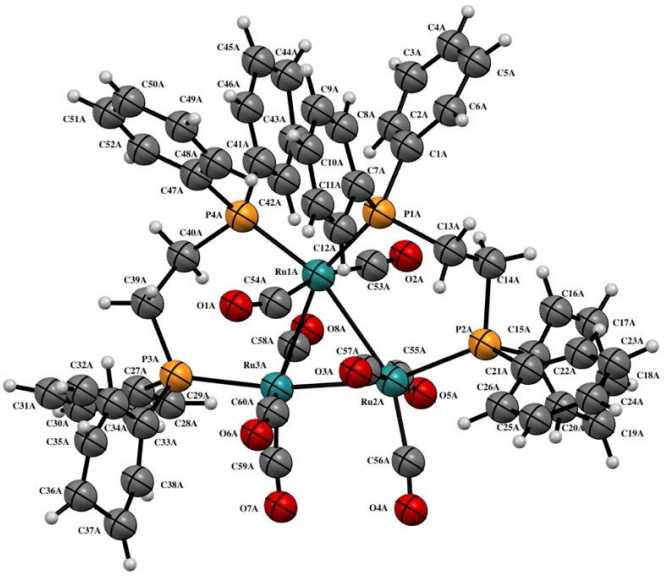

(a)

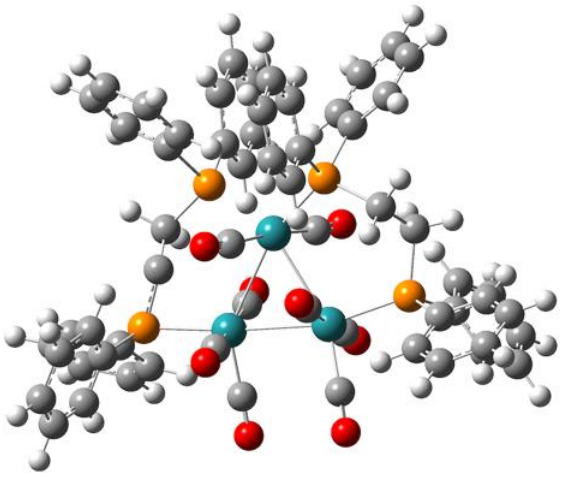

(b)

Figure 1. (a) ORTEP diagram of $Ru_3(CO)_8(\mu\text{-}Ph_2PCH_2CH_2PPh_2)_2$ showing thermal ellipsoids at the 50% probability level. (b) Optimised structure of $Ru_3(CO)_8(\mu\text{-}Ph_2PCH_2CH_2PPh_2)_2$ at LanL2DZ for Ru metal and B3LYP/6-31G (d, p) basis set for all other atoms The visualisation was carried out using only one molecule. The other molecule in the unit cell had been omitted for clarity.

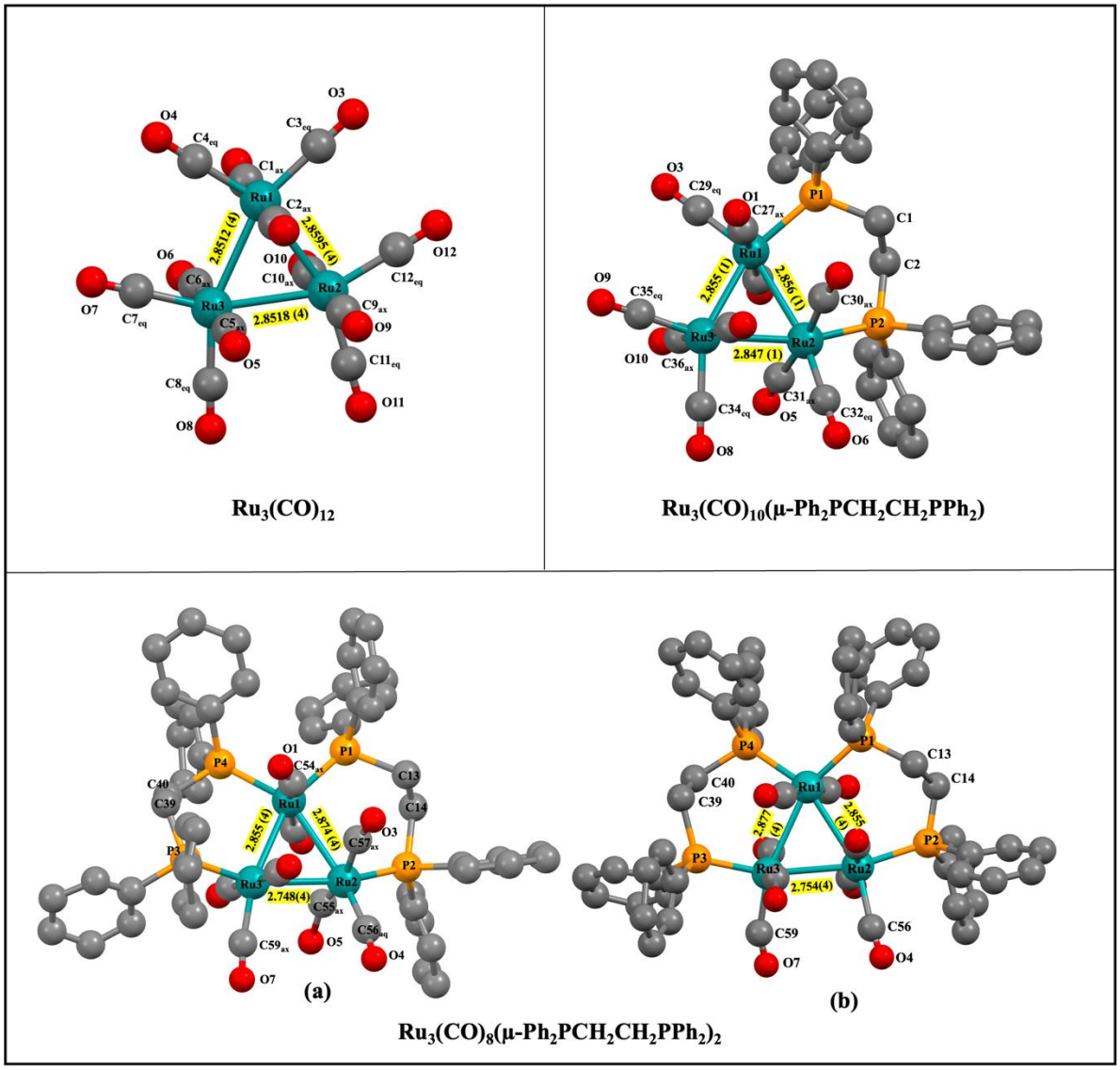

Figure 2. The bond length for Ru–Ru bonds in $Ru_3(CO)_{12}$, $Ru_3(CO)_{10}(\mu\text{-}Ph_2PCH_2CH_2PPh_2)$, and $Ru_3(CO)_8(\mu\text{-}Ph_2PCH_2CH_2PPh_2)_2$ (a) molecule A; (b) molecule B. Hydrogen atoms have been omitted for clarity.

Besides, the substitution of CO ligands by $Ph_2PCH_2CH_2PPh_2$ in $Ru_3(CO)_{12}$ causes the ranges of Ru–Ru–Ru bond angle to progressively decrease $Ru_3(CO)_{12}$ [59.90-60.18°] [22], $Ru_3(CO)_{10}(\mu\text{-}Ph_2PCH_2CH_2PPh_2)$ [59.81-60.13°] [9], and $Ru_3(CO)_8(\mu\text{-}Ph_2PCH_2CH_2PPh_2)_2$ [57.44-61.69°], as shown in Figure 3. With regards to the intracyclic Ru–Ru–P bond angles for $Ru_3(CO)_8(\mu\text{-}Ph_2PCH_2CH_2PPh_2)_2$, Ru2–Ru1–P1 and Ru3–Ru1–P4 has a small value compared to the Ru1–Ru2–P2 and Ru1–Ru3–P3. The smaller bond angle of Ru2–Ru1–P1 and Ru3–Ru1–P4 might be due to the strain imposed on Ru1 that is attached to two bidentate ligands of $Ph_2PCH_2CH_2PPh_2$. The Ru–Ru–P bond angle differences are not significantly observed in $Ru_3(CO)_{10}(\mu\text{-}Ph_2PCH_2PPh_2)$ [Ru2–Ru1–P1= 96.7°; Ru1–Ru2–P2= 90.2°; Ru1–Ru2–P3= 92.5°] [23] and $Ru_3(CO)_8(\mu\text{-}Ph_2PCH_2PPh_2)_2$ [Ru2–Ru1–P1=95.5(1)°; Ru1–Ru2–P2= 89.4(1)°] [4], as shown in Figure 3. They have relatively similar values. The distribution of axial carbonyl (Figure 4) demonstrates that bond angles of axial carbonyl in the compound ranges at 163.03-168.25(2)° (molecule A) and 160.23-169.41(2)° (molecule B); this is considered far from the linearity compared to $Ru_3(CO)_{10}(\mu\text{-}Ph_2PCH_2CH_2PPh_2)$ [172.51-174.06°] [9], and $Ru_3(CO)_{12}$ [177.21-179.27°] [22].

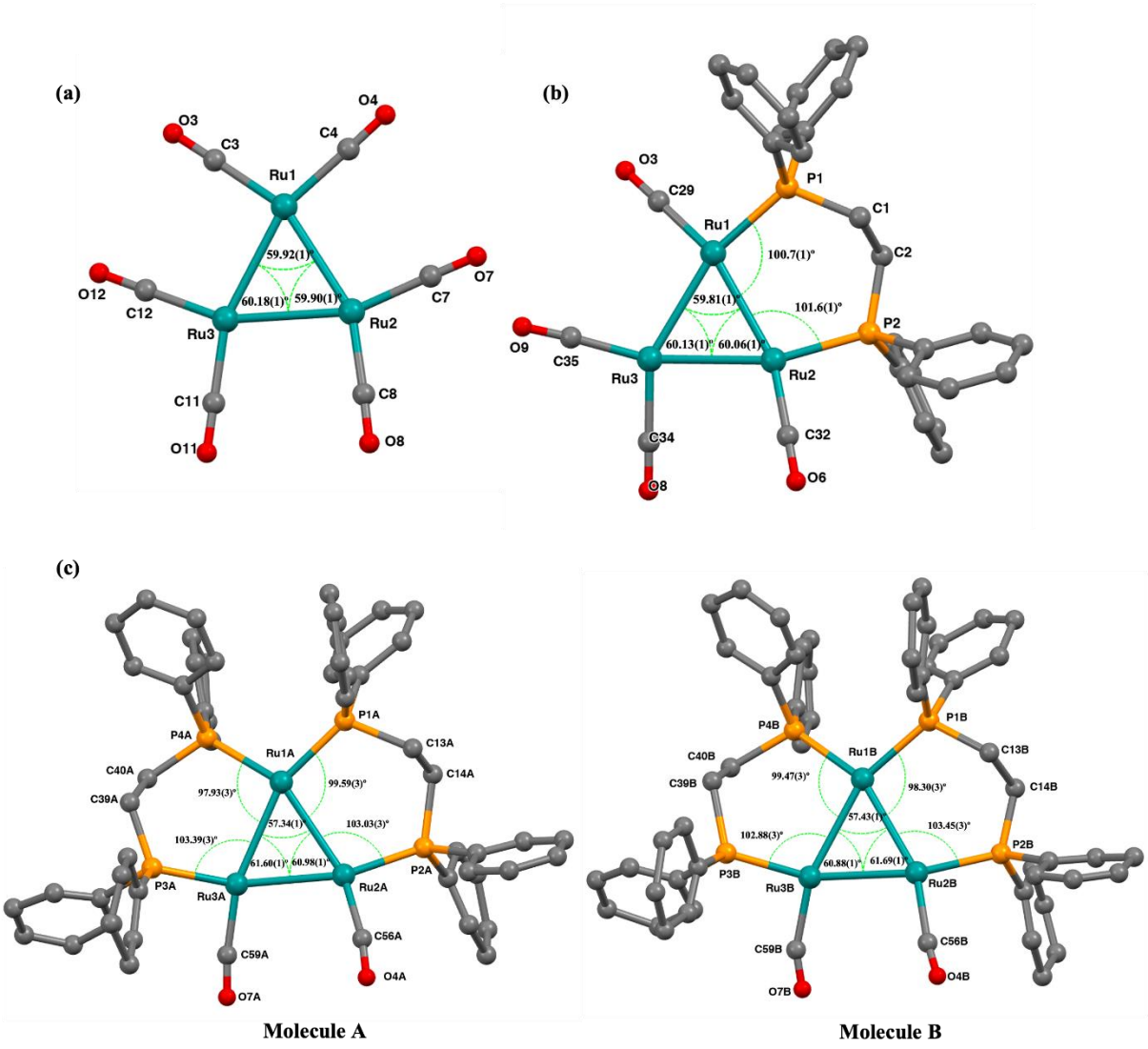

Figure 3. Ru–Ru–Ru bond lengths and the distribution of equatorial ligands in (a) $Ru_3(CO)_{12}$ (b) $Ru_3(CO)_{10}(\mu\text{-}Ph_2PCH_2CH_2PPh_2)$ (c) $Ru_3(CO)_8(\mu\text{-}Ph_2PCH_2CH_2PPh_2)_2$.

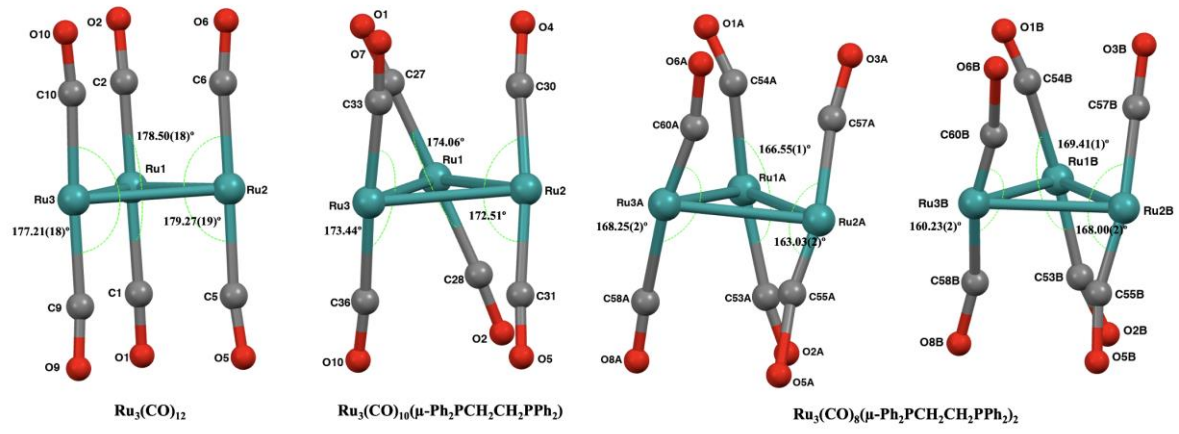

Figure 4. Distribution of axial carbonyl ligands in $Ru_3(CO)_{12}$, $Ru_3(CO)_{10}(\mu\text{-}Ph_2PCH_2CH_2PPh_2)$, and $Ru_3(CO)_8(\mu\text{-}Ph_2PCH_2CH_2PPh_2)_2$.

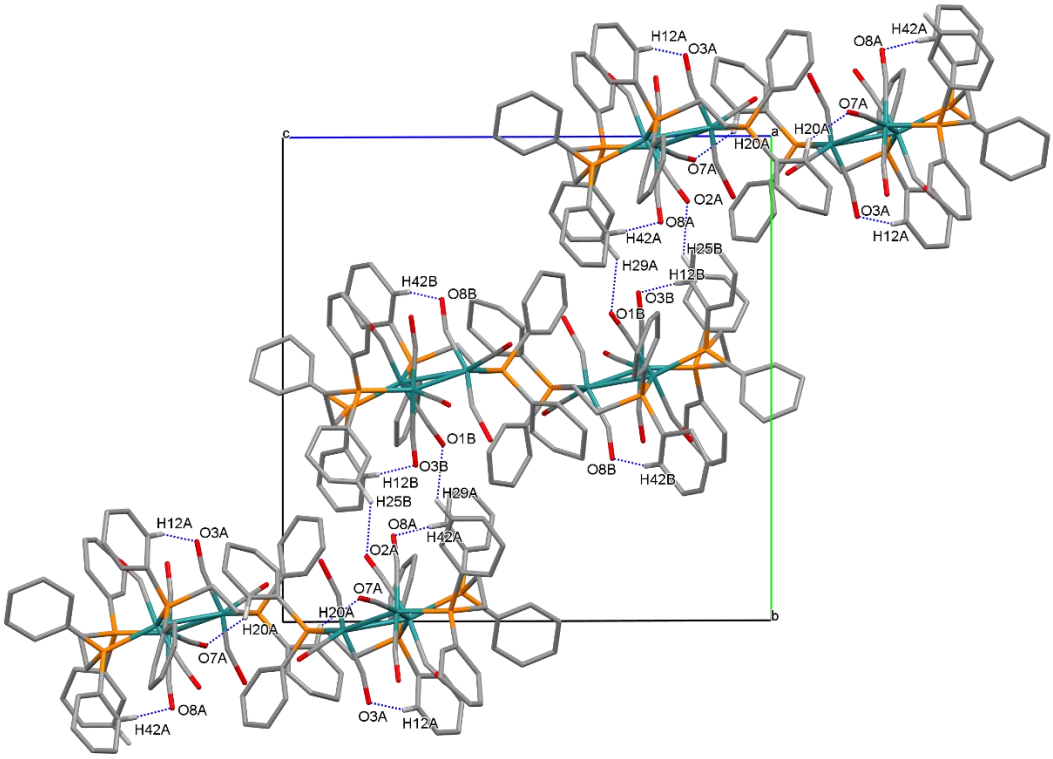

Figure 5. Crystal packing diagram of $Ru_3(CO)_8(\mu\text{-}Ph_2PCH_2CH_2PPh_2)_2$, viewed down the *a*-axis. Hydrogen atoms are omitted for clarity. The hydrogen bonds are indicated by the blue dashed line.

Table 2. Hydrogen bonds for $Ru_3(CO)_8(\mu\text{-}Ph_2PCH_2CH_2PPh_2)_2$.

D–H···A	D–H (Å)	H···A (Å)	D···A (Å)	D–H···A (°)
C12A–H12A···O3A	0.93	2.46	3.38(4)	167
C12B–H12B···O3B	0.93	2.46	3.39(4)	176
C20A–H20A···O7A^{i}	0.93	2.56	3.36(4)	144
C25B–H25B···O2A^{ii}	0.93	2.28	3.06(4)	141
C29A–H29A···O1B^{ii}	0.93	2.29	3.02(4)	135
C42A–H42A···O8A	0.93	2.49	3.41(4)	171
C42B–H42B···O8B	0.93	2.44	3.36(4)	167

(Symmetry codes : i = -x,2-y,2-z ; ii = -1+x,y,z)

In the crystal packing, the molecules of $Ru_3(CO)_8(\mu\text{-}Ph_2PCH_2CH_2PPh_2)_2$ were stacked-up diagonally across the *b*/*c*-axis, which formed a stair-like motif (Figure 5) when viewed down the *a*-axis. These molecules were stabilised by a three-dimensional network of C–H·O intra- and intermolecular hydrogen bonds (Table 2). From Table 1, this crystal has a high R_{int} value (25.16). A few attempts to grow good crystals suitable for Single Crystal X-ray Diffraction analysis with low value of R_{int} were conducted and unsuccessful. However, in this work, we emphasised on validation of the molecular structure of $Ru_3(CO)_8(\mu\text{-}Ph_2PCH_2CH_2PPh_2)_2$ because there is no crystal structure reported for this compound despite the fact that Bruce and co-workers had provided information on the method of synthesis and prediction of the structure by spectroscopic characterisation [9].

DFT Studies

The DFT optimised structure of $Ru_3(CO)_8(\mu\text{-}Ph_2PCH_2CH_2PPh_2)_2$ is shown in Figure 1. (b). The DFT investigation was performed by optimising the geometry structure as the first procedure toward the structure of $Ru_3(CO)_8(\mu\text{-}Ph_2PCH_2CH_2PPh_2)_2$. This is crucial to determine the lowest energy configuration for $Ru_3(CO)_8(\mu\text{-}Ph_2PCH_2CH_2PPh_2)_2$. The comparison of some bond lengths and angles *via* the experimental (Single crystal XRD) and the

theoretical (DFT) methods were conducted and listed in Table 3. In order to assess the significance of the performed DFT method, the calculated values of these geometry parameters acquired by DFT method are plotted against the experimental results obtained by the single crystal X-ray diffraction analysis. The correlation coefficients (R^2) are crucial to determine the reliability of the result. From the graph in Figure 6, The R^2 values vary in a consistent pattern. R^2 is considered inadequate with a value of 0.6846 for molecule A and 0.6822 for molecule B. This could be due to low quality crystal data or the chosen basis set employed in the optimised structure is not compatible or suitable to the structure type, despite the fact that this basis set is widely used for many metal cluster optimisation [24-25].

Table 3. Selected bond lengths and bond angles of $Ru_3(CO)_8(\mu\text{-}Ph_2PCH_2CH_2PPh_2)_2$.

Bond Length	Experimental (Å)		DFT (Å)
	Molecule A	Molecule B	
Ru1–Ru2	2.874(4)	2.855(4)	2.946
Ru1–Ru3	2.855(4)	2.877(4)	3.030
Ru2–Ru3	2.748(4)	2.754(4)	2.933
Ru1–P1	2.273(10)	2.302(10)	2.442
Ru1–Ru4	2.308(10)	2.296(9)	2.398
Ru2–P2	2.246(9)	2.270(10)	2.400
Ru3–P3	2.264(9)	2.244(10)	2.387
Ru1–$C53_{ax}$	1.95(4)	1.86(4)	1.156
Ru1–$C54_{ax}$	1.97(4)	1.99(4)	1.164
Ru2–$C55_{ax}$	1.39(3)	1.64(4)	1.154
Ru2–$C57_{ax}$	1.85(4)	1.88(4)	1.165
Ru2–$C56_{eq}$	1.87(3)	1.99(4)	1.158
Ru2–$C58_{eq}$	1.94(4)	1.77(4)	1.160
Ru2–$C59_{ax}$	1.83(4)	1.90(3)	1.157
Ru3–$C60_{ax}$	1.54(4)	1.40(4)	1.152
P1–C7	1.84(4)	1.82(4)	1.856
P1–C13	1.92(3)	1.86(3)	1.860
P1–C1	1.73(3)	1.87(4)	1.878
P1–C27	1.91(4)	1.83(4)	1.842
P1–C33	1.69(3)	1.75(4)	1.829
P1–C39	1.76(3)	1.92(3)	1.704
P4–C41	1.87(4)	1.89(4)	1.857
P4–C47	1.824(18)	1.72(3)	1.854
P4–C40	1.85(3)	1.91(3)	1.877
P2–C14	1.89(3)	1.75(3)	1.704
P2–C15	1.77(4)	1.68(4)	1.829
P2–C21	1.79(4)	1.85(3)	1.842

Bond Angle	Experimental (Å)		DFT (Å)
	Molecule A	Molecule B	
Ru3–Ru1–Ru2	57.34(1)	57.43(1)	58.756
Ru1–Ru2–Ru3	60.98(1)	61.69(1)	62.046
Ru2–Ru3–Ru1	61.60(1)	60.88(1)	59.198
Ru3–Ru1–P4	97.93(3)	99.47(3)	156.889
Ru1–Ru3–P3	103.39(3)	102.88(3)	114.605
Ru2–Ru1–P1	99.59(3)	98.30(3)	151.035
Ru1–Ru2–P2	103.03(3)	103.45(3)	102.706
P1–Ru1–P4	106.14(3)	105.82(3)	106.926
$C56_{eq}$–Ru2–P2	98.45(1)	98.10(1)	97.848
$C59_{eq}$–Ru3–P3	94.33(1)	95.72(1)	99.213
$C60_{ax}$–Ru3–$C58_{ax}$	168.25(2)	160.23(2)	172.009
$C54_{ax}$–Ru1–$C53_{ax}$	166.55(1)	169.41(1)	174.050
$C57_{ax}$–Ru2–$C55_{ax}$	163.03(2)	168.00(2)	170.432
Ru2–$C56_{eq}$–O4	171(3)	173(3)	177.026
Ru3–$C59_{eq}$–O7	172(3)	160(3)	176.053

Ru1–$C54_{ax}$–O1	155(3)	170(3)	175.322
Ru1–$C53_{ax}$–O2	171(3)	166(3)	174.203
Ru2–$C53_{ax}$–O3	167(3)	169(3)	169.178
Ru2–$C55_{ax}$–O5	159(3)	165(3)	173.855
Ru3–$C60_{ax}$–O6	165(3)	159(3)	174.257
Ru3–$C58_{ax}$–O8	170(3)	158(3)	173.795
Ru2–Ru3–$C60_{ax}$	75.5(12)	76.2(13)	82.537
Ru3–Ru1–$C54_{ax}$	81.3(10)	74.6(9)	79.612
Ru2–Ru3–$C58_{ax}$	95.1(9)	89.8(11)	92.542
Ru2–Ru1–$C53_{ax}$	74.8(10)	81.3(10)	77.570
Ru2–Ru1–$C54_{ax}$	91.8(10)	91.2(9)	97.506
Ru3–Ru2–$C57_{ax}$	91.6(10)	94.8(15)	82.189
Ru3–Ru1–$C53_{ax}$	91.6(10)	94.9(10)	94.879
Ru3–Ru2–$C55_{ax}$	76.2(12)	75.3(11)	82.189
Ru1–Ru2–$C57_{ax}$	72.6(10)	77.9(10)	73.344

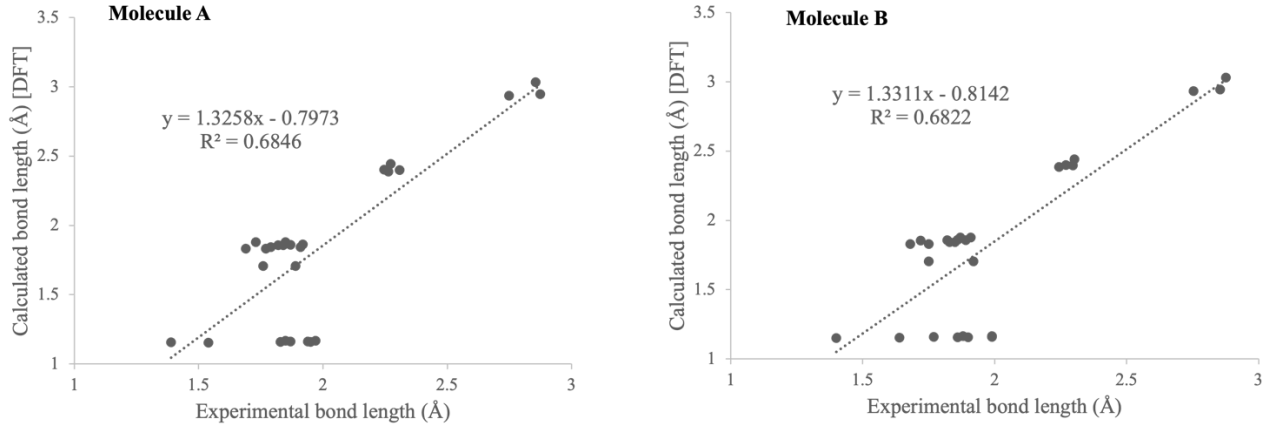

Figure 6. Plot of experimental bond length (single crystal X-ray diffraction) and calculated bond length (DFT) for (a) molecule A and (b) molecule B of $Ru_3(CO)_8(\mu\text{-}Ph_2PCH_2CH_2PPh_2)_2$.

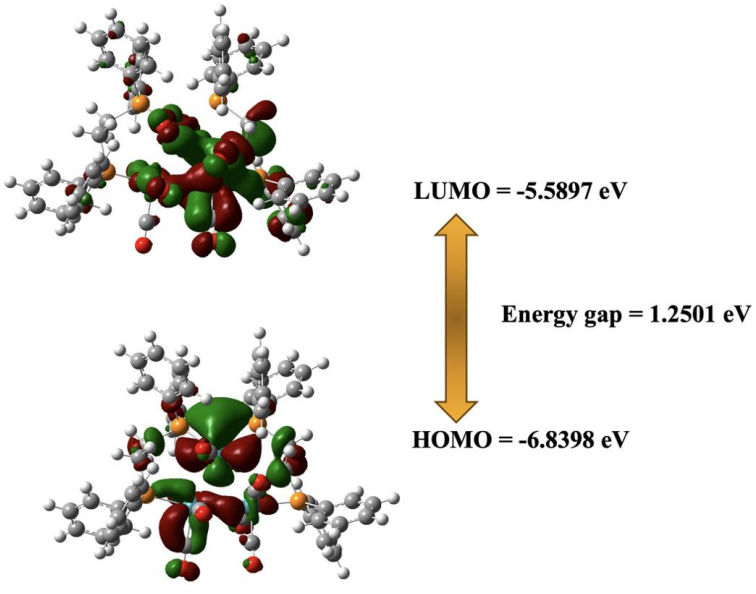

Figure 7. HOMO and LUMO orbitals of $Ru_3(CO)_8(\mu\text{-}Ph_2PCH_2CH_2PPh_2)_2$.

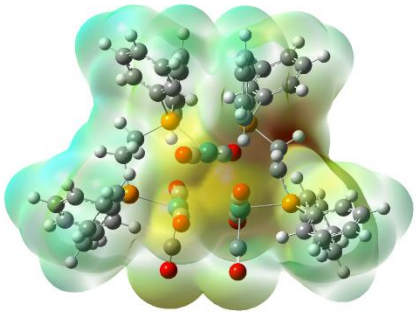

Figure 8. Molecular electrostatic potential surface of $Ru_3(CO)_8(\mu\text{-}Ph_2PCH_2CH_2PPh_2)_2$.

In the Frontier Molecular Orbitals, the Highest Occupied Molecular Orbital (HOMO) and Lowest Occupied Molecular Orbital (LUMO) are important in presenting the electron density distribution for the molecular orbitals of $Ru_3(CO)_8(\mu\text{-}Ph_2PCH_2CH_2PPh_2)_2$. Hard molecules are those with a large energy gap, whereas soft molecules are those with a small energy gap. Compared to soft molecules, hard molecules are less polarizable and require more energy for excitation [26]. The energy gap between the HOMO and LUMO of the compound was measured to be 1.2501 eV. Figure 7 depicts a visualisation of the HOMO-LUMO energy gap. The HOMO orbitals in the figure are scattered around the ruthenium centre atoms, and some at the methylene group. In the case of LUMO, the electron density was concentrated in the triangle region of the metal center and at the carbonyl part of the structure. The HOMO and LUMO distributions are nearly identical. The HOMO, on the other hand, is more spread across the structure, whereas the LUMO is more prominent on one side.

To forecast the reactive sites of $Ru_3(CO)_8(\mu\text{-}Ph_2PCH_2CH_2PPh_2)$, the molecular electrostatic potential (MEP) is calculated using the electron density of the compound. This was conducted using the DFT method of study. The MEP map, as shown in Figure 8, significantly shows the electrophilic and nucleophilic regions which are indicated by different codes of colour. The white regions represent the neutral part of the structure, while the blue and red colours show the electrophilic and nucleophilic regions of the structure, respectively. The molecule electrostatic potential in the MEP diagram ranges from -0.138 to 0.138 a.u. The electrostatic potentials increase from red to blue, with the red-coloured region representing the negative site.

CONCLUSION

In summary, this work describes the synthesis and characterisation of a triruthenium cluster derivative, $Ru_3(CO)_8(\mu\text{-}Ph_2PCH_2CH_2PPh_2)_2$ by using sodium benzophenone ketyl as an initiator to induce the substitution of carbonyl by $Ph_2PCH_2CH_2PPh_2$ ligand. The crystal structure of $Ru_3(CO)_8(\mu\text{-}Ph_2PCH_2CH_2PPh_2)_2$ was successfully obtained. The molecular structure of $Ru_3(CO)_8(\mu\text{-}Ph_2PCH_2CH_2PPh_2)_2$ in this study aligns with the previously proposed structure, in which both of the $Ph_2PCH_2CH_2PPh_2$ ligands are bonded in $\mu_2\text{-}\eta^2$ mode to the Ru−Ru bonds [9]. The theoretical and experimental geometric parameter findings exhibit a consistent pattern of deviation in their values. According to the Frontier Molecular Orbital analysis, the energy gap of HOMO-LUMO for this molecule is 1.2501 eV. The quality of the crystal data could be improved by growing a good quality of crystal that is suitable for Single Crystal X-ray diffraction analysis.

ACKNOWLEDGEMENTS

The authors are grateful to the Organic Synthesis Research Laboratory, Institute of Science (IOS), UiTM Kampus Puncak Alam, for the research facilities. We also acknowledged the Ministry of Higher Education, Malaysia, under the Fundamental Research Grant Scheme (FRGS) (Project Number: FRGS/1/2021/STG04/UITM/02/4) for financial support. We also would like to convey our special gratitude to the Center of Information and Communication Technology (CICT), Universiti Teknologi Malaysia (UTM) for supporting and providing facilities of high – performance computer maintained by the grant [FRGS, Vot R.J130000.7854.5F471]

Supplementary Data

CCDC2297431 contains the supplementary crystallographic data for this paper. These data can be obtained free of charge at www.ccdc.cam.ac.uk/consts/retrieving.html (or from the Cambridge Crystallographic data centre (CCDC), 12, Union Road, Cambridge CB2 IE2, UK, Fax: C44 (0)1223- 336033; email-deposit@ccdc.cam.ac.uk).

REFERENCES

1. Böttcher, H. C. and Heinemann, J. (2021) Electron-Deficient Triruthenium Clusters Containing Small Bite-Angle PNP-Ligands. *Zeitschrift für*

anorganische und allgemeine Chemie, **647(8)**, 876–880.

2. Bhowmik, M. L., Al Mamun, M. A., Ghosh, S., Nesterov, V. N., Richmond, M. G., Kabir, S. E. and Roesky, H. W. (2023) Polynuclear ruthenium clusters containing stibine, stibene, and stibinidene ligands. *Journal of Organometallic Chemistry*, **984**, 122574.

3. Mikeska, E. R., Powell, C. B. and Powell, G. L. (2021) Triosmium Carbonyl Clusters Containing a Mixture of Dppm and Dppe Ligands. *Journal of Chemical Crystallography*, **51**, 457–464.

4. Lavigne, G., Lugan, N. and Bonnet, J. J. (1982) Structural characterization of a substituted derivative of $Ru_3(CO)_{12}$: 1, 2; 3, 1-bis{μ-[bis (diphenylphosphino)methane]-*P, P'*}-1,1,2,2,2,3,3, 3-octacarbonyl-triangulo-triruthenium (0) acetone solvate. *Acta Crystallographica Section B: Structural Crystallography and Crystal Chemistry*, **38(7)**, 1911–1916.

5. Sánchez-Cabrera, G., García-Báez, E. V. and Rosales-Hoz, M. J. (2000) The reaction of [$Ru_3(CO)_{12}$] with bis (diphenylphosphino) amine. The crystal and molecular structure of [$Ru_3(CO)_{10}$(dppa)] and [$Ru_3(CO)_8$(dppa)$_2$]. *Journal of Organometallic Chemistry*, **599(2)**, 313–316.

6. Diz, E. L., Neels, A., Stoeckli-Evans, H. and Süss-Fink, G. (2001) New $Ru_3(CO)_{12}$ derivatives with bulky diphosphine ligands: synthesis, structure and catalytic potential for olefin hydroformylation. *Polyhedron*, **20(22-23)**, 2771–2780.

7. Fontal, B., Hernández, R., Suárez, T., Reyes, M. and Bellandi, F. (1999) Catalysis studies of $Ru_3(CO)_{12}$ substituted with $PPh_2CH_2CH_2CH_2PPh_2$. *Revista Tecnica de la Facultad de Ingenieria Universidad del Zulia*, **22(2)**, 79–89.

8. Cesari, C., Shon, J. H., Zacchini, S. and Berben, L. A. (2021) Metal carbonyl clusters of group 8-10: synthesis and catalysis. *Chemical Society Reviews*, **50(17)**, 9503–9539.

9. Bruce, M. I., Hambley, T. W., Nicholson, B. K. and Snow, M. R. (1982) Cluster chemistry: X. Preparation of 1,2-bis(diphenylphosphino) ethane derivatives of $Ru_3(CO)_{12}$: crystal and molecular structures of $Ru_3(CO)_{10}(\mu\text{-}PH_2PCH_2CH_2PPh_2)$. *Journal of Organometallic Chemistry*, **235(1)**, 83–91.

10. Bruker (2021) *APEX4 and SAINT*. Bruker AXS Inc., Madison, Wisconsin, USA.

11. Dolomanov, O. V., Bourhis, L. J., Gildea, R. J., J. Howard, A. K. and Puschmann, H. (2009) OLEX2: a complete structure solution, refinement and analysis program. *Journal of Applied Crystallography*, **42(2)**, 339–341.

12. Sheldrick, G. M. (2008) A short history of SHELX. *Acta Crystallographica Section A: Foundations of Crystallography*, **64(1)**, 112–122.

13. Sheldrick, G. M. (2015) Crystal structure refinement with SHELXL. *Acta Crystallographica Section C: Structural Chemistry*, **71(1)**, 3–8.

14. Macrae, C. F., Sovago, I., Cottrell, S. J., Galek, P. T. A., McCabe, P., Pidcock, E., Platings, M., Shields, G. P., Stevens, J. S., Towler, M. and Wood, P. A. (2020) Mercury 4.0: from visualization to analysis, design and prediction. *Journal of applied crystallography*, **53(1)**, 226–235.

15. Spek, A. L. (2009) Structure validation in chemical crystallography. *Acta Crystallographica Section D: Biological Crystallography*, **65(2)**, 148–155.

16. Frisch, M. J., Trucks, G. W., Schlegel, H. B., Scuseria, G. E., Robb, M. A., Cheeseman, J. R., Scalmani, G., Barone, V., Mennucci, B., Petersson, G. A., Nakatsuji, H., Caricato, M., Li, X., Hratchian H. P., Izmaylov, A. F., Bloino, J., Zheng, G., Liang, W., Hada, M., Ehara, M., Toyota, K., Fukuda, R., Hasegawa, J., Ishida, M., Nakajima, T., Honda, Y., Kitao, O., Nakai, H., Vreven, T., Throssell, K., Montgomery, J. A., Peralta, J. E., Ogliaro, F., Bearpark, M. J., Heyd, J. J., Brothers, E. N., Kudin, K. N., Staroverov, V. N., Keith, T. A., Kobayashi, R., Normand, J., Raghavachari, K., Rendell, A. P., Burant, J. C., Iyengar, S. S., Tomasi, J., Cossi, M., Millam, J. M., Klene, M., Adamo, C., Cammi, R., Ochterski, J. W., Martin, R. L., Morokuma, K., Farkas, O., Foresman, J. B. and Fox, D. J. (2016) Gaussian 16 (Revision C. 01), Gaussian, Inc. Wallingford CT.

17. Roy, D., Todd, K. and John, M. (2009) Gauss View, Ver 5.0.9, Semichem Inc.

18. Becke, A. D. (1993) Density-functional thermos-chemistry. III. The role of exact exchange. *The Journal of Chemical Physics*, **98(7)**, 5648–5652.

19. Lee, C., Yang, W. and Parr, R. G. (1988) Development of the Colle-Salvetti correlation-energy formula into a functional of the electron density. *Physical Review B: Condensed Matter Materials Physics*, **37(2)**, 785–789.

20. Hay, P. J. and Wadt, W. R. (1985) *Ab initio* effective core potentials for molecular calculations. Potentials for K to Au including the outermost core orbitals. *The Journal of Chemical Physics*, **82(1)**, 299–310.

21. Wadt, W. R. and Hay, P. J. (1985) *Ab initio* effective core potentials for molecular calculations.

Potentials for main group elements Na to Bi. *The Journal of Chemical Physics*, **82(1)**, 284–298.

22. Mason, R. and Rae, A. I. M. (1968) The crystal structure of ruthenium carbonyl, $Ru_3(CO)_{12}$. *Journal of the Chemical Society A: Inorganic, Physical, Theoretical*, 778–779.

23. Coleman, A. W., Jones, D. F., Dixneuf, P. H., Brisson, C., Bonnet, J. J. and Lavigne, G. (1984) Dehalogenation of binuclear arene-ruthenium complexes: a new route to homonuclear triruthenium and heteronuclear ruthenium-iron cluster complexes containing chelating phosphorus ligands. Crystal structure of $Ru_3(CO)_{10}(Ph_2PCH_2PPh_2)$. *Inorganic Chemistry*, **23(7)**, 952–956.

24. Barolo, C., Nazeeruddin, M. K., Fantacci, S., Di Censo, D., Comte, P., Liska, P., Viscardi, G., Quagliotto, P., Angelis, F. D. and Grätzel, M. (2006) Synthesis, characterization, and DFT-TDDFT computational study of a ruthenium complex containing a functionalized tetradentate ligand. *Inorganic chemistry*, **45(12)**, 4642–4653.

25. Cabeza, J. A., del Río, I., Miguel, D., Pérez-Carreño, E. and Sánchez-Vega, M. G. (2008) Reactivity of N-Heterocyclic Carbenes with $[Ru_3(CO)_{12}]$ and $[Os_3(CO)_{12}]$. Influence of Ligand Volume and Electronic Effects. *Organometallics*, **27(2)**, 211–217.

26. Verma, V. K., Guin, M., Solanki, B. and Singh, R. C. (2020) Molecular structure, HOMO and LUMO studies of Di(Hydroxybenzyl) diselenide by quantum chemical investigations. *Materials Today: Proceedings*, **49(8)**, 3200–3204.